IL NUOVO CIMENTO Vol. 29 C, N. 2 Marzo-Aprile 2006
DOI 10.1393/ncc/i2005-10196-y

Effect of different spectral distributions to image a contrast detail phantom in the mammography energy range

U. Bottigli([1])([2]), B. Golosio([1])([2]), G. L. Masala([1])([2]), P. Oliva([1])([2])(*), S. Stumbo([1])([2]), A. Bravin([3]), A. Bacci([4]), L. Serafini([4]), C. Maroli([4])([5]), V. Petrillo([4])([5]), M. Ferrario([6]) and C. Vaccarezza ([6])

([1]) *Struttura Dipartimentale di Matematica e Fisica, Università di Sassari - Sassari, Italy*
([2]) *INFN, Sezione di Cagliari - Cagliari, Italy*
([3]) *European Synchrotron Radiation Facility - Grenoble, France*
([4]) *INFN, Sezione di Milano - Milano, Italy*
([5]) *Università di Milano - Milano, Italy*
([6]) *INFN, Laboratori Nazionali di Frascati - Frascati, Italy*

(ricevuto il 12 Ottobre 2005; revisionato il 9 Dicembre 2005; approvato il 15 Dicembre 2005; pubblicato online il 16 Febbraio 2006)

Summary. — Traditionally X-ray sources used in mammography are X-ray tubes. Synchrotron radiation sources have shown better imaging performances, but they cannot replace conventional X-ray tube systems in routine mammographic examinations. A new generation of quasi-monochromatic, high-flux X-ray sources is currently under development, based on Thomson backscattering of photons produced by a laser on a highly focused electron beam. They offer important potential applications in the medical field. In this work, we will discuss an application in the field of mammography, by using a Monte Carlo code, in which the effect of different spectral distributions and different mean energies on the image quality is studied. A test object, consisting of a block of Polymethyl Methacrylate (PMMA) containing air-filled holes (Contrast Detail Phantom) is used for the simulations. Results show 1–2 keV of energy spread for a quasi-monochromatic source produce images whose quality is comparable within 3–4% with those obtained by monochromatic sources and whose visibility is dramatically enhanced with respect to images obtained with X-ray tubes.

PACS 87.59.Ek – Mammography.

1. – Introduction

It is known that in breast radiography the best image quality is obtained when photons have energies around 20 keV [1] if the dose to the patient is kept constant. In fact, the photons having lower energies are highly absorbed by the patient, while those having higher energies yield a low contrast.

(*) E-mail: oliva@uniss.it

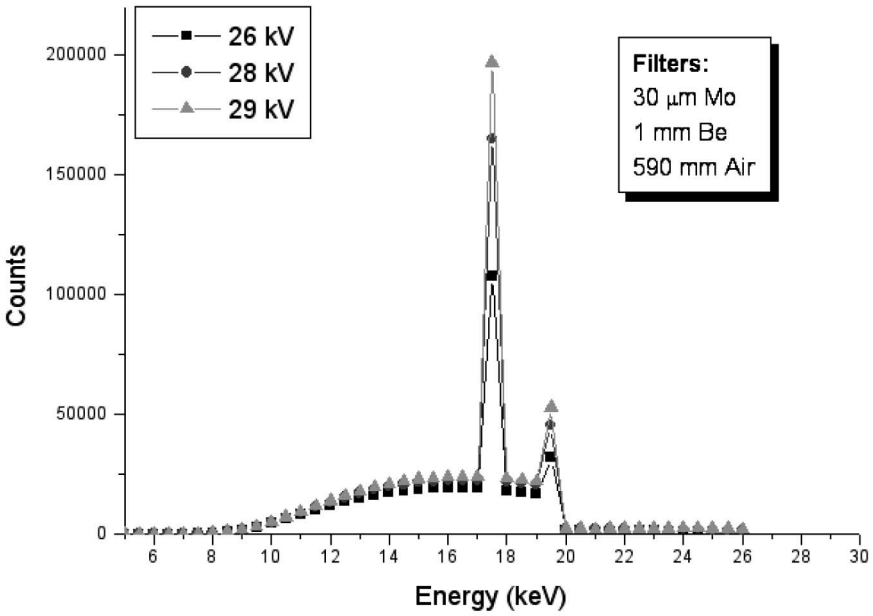

Fig. 1. – Some typical spectra used in mammography. All data are generated using IPEM catalog [2].

The traditional X-ray sources used in mammography are X-ray tubes, the most common one being a molybdenum (Mo) anode, used at 26–32 kV voltages. Additional filters usually are 1 mm Be and 25–30 μm Mo. In fig. 1, some typical mammography spectra generated by a catalog provided by The Institute of Physics and Engineering in Medicine (IPEM) [2], are reported. Tube voltage is set in order to obtain the required mean energy value. However, the energy spectrum of conventional X-ray tube systems used for mammography is polychromatic, even after filtration it shows a significant number of photons in the whole range between 10 and 25 keV.

Synchrotron radiation (SR) sources can provide highly monochromatic, energy tunable radiation. Different imaging techniques based on the properties of SR have been applied to the medical field, *e.g.*, conventional full-field imaging with monochromatic radiation, phase contrast imaging and diffraction enhanced imaging [3-5]. The advantages of such techniques regarding conventional X-ray tube systems have been widely proven in various literature. However, due to high costs, limited beam-time and practical problems, synchrotrons cannot replace conventional X-ray tube systems in routine mammographic examinations.

A new generation of quasi-monochromatic, high-flux X-ray sources that are currently under development, is based on Thomson backscattering of photons produced by a laser on a highly focused electron beam [6-8]. These sources can be in perspective much more compact and less expensive than synchrotrons and are capable to produce synchronized radiation pulses shorter than a picosecond. Even though these sources cannot yield a flux as high as that of synchrotrons, they present a good compromise between high flux/monochromaticity and compactness. They have important potential applications in the medical field and particularly in mammography.

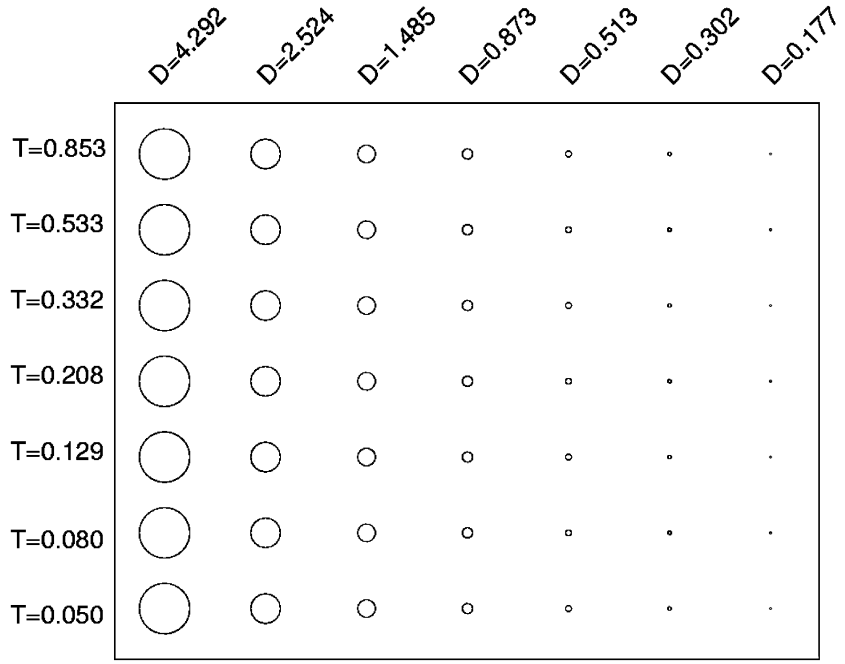

Fig. 2. – Schematic view of Contrast Detail Phantom. Diameter (D) and thickness (T) dimensions are in millimeters.

The aim of this work is to study how different energy spectra affect image quality in mammography. To reach this scope, we ran a set of Monte Carlo simulations in which all the parameters but the energy spectra are kept constant. Contrast and Signal-to-Noise Ratio (SNR) are evaluated for monochromatic, quasi-monochromatic and polychromatic sources.

In particular, some indications on working parameters for a quasi-monochromatic source are provided.

2. – Methods

In order to evaluate the effect of different X-ray energy spectra in mammography, we ran a set of Monte Carlo simulations.

A Monte Carlo code for the simulation of X-ray imaging and spectroscopy experiments in heterogeneous samples was used [9]. The energy spectrum, polarization and profile of the incident beam can be defined so that X-ray tube systems, as well as synchrotron sources can be simulated. Either a single-element or an array detector can be modeled in the simulation. The sample can have arbitrary geometry and composition, which can be modeled by giving the elemental weight fractions and mass density in each voxel of a 3D regular grid or in a collection of geometric shapes. Photoelectric absorption, fluorescent emission, elastic and inelastic scattering are included in the simulation.

In order to reduce the computational time, we exploited the use of so-called variance reduction techniques, which basically consist in forcing each event into an interesting final channel (*e.g.*, a signal can only be produced when at least one photon trajectory ends

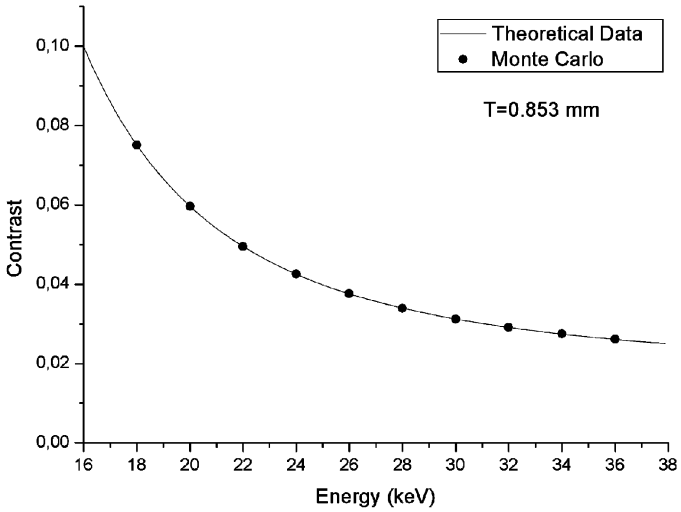

Fig. 3. – Comparison between theoretical contrast and Monte Carlo calculated contrast, for monochromatic beams, for the 0.853 mm thickness detail, as a function of energy. Error bars for Monte Carlo calculated contrast are not shown since they are too small for the scale of the graphic.

up in a detector pixel) and assigning the event a weight fraction equal to the probability associated to the channel itself [10, 11].

To concentrate the analysis on the mammographic imaging dependence on X-ray spectral distributions, we used the same geometry in all the simulations. The X-ray source was a point-like one and the source-detector distance was 100 m, in order to make incident X-rays practically parallel.

Several X-ray spectra were simulated:

– monochromatic spectra, from 18 keV to 36 keV, step 2 keV, that simulate synchrotron radiation.

– Quasi-monochromatic spectra, that simulate Thomson back-scattering source. Gaussian shapes were used, centered at 22 keV, 26 keV and 30 keV and with a standard deviation of 1, 2, 3, 4, 5, 7 and 10 keV.

– Polychromatic spectra, that simulate those produced by mammography X-ray tubes. They were generated using IPEM [2] with the following parameters: Mo anode, anode inclination 12° and additional filtration of 0.03 mm of Mo, 1 mm of Be, 650 mm of air. As anode voltage we used 26, 28, 30 and 32 kV.

The incident fluence was the same for all the configurations. It was calculated using IPEM catalog [2] with parameter values that are reasonable for a mammography examination. These parameters were 28 kV of anodic voltage, 12° of anode angle, 60 mAs of exposure. Additional filtrations 0.03 mm of Mo, 1 mm of Be and 650 mm of air were used, supposing a tube-detector distance of 650 mm. The resulting fluence was $\Phi = 2.72 \times 10^7 \gamma/\mathrm{mm}^2$. The mean glandular dose (MGD) was estimated using data derived by Boone [12] for the normalized glandular dose and for the exposure per unit

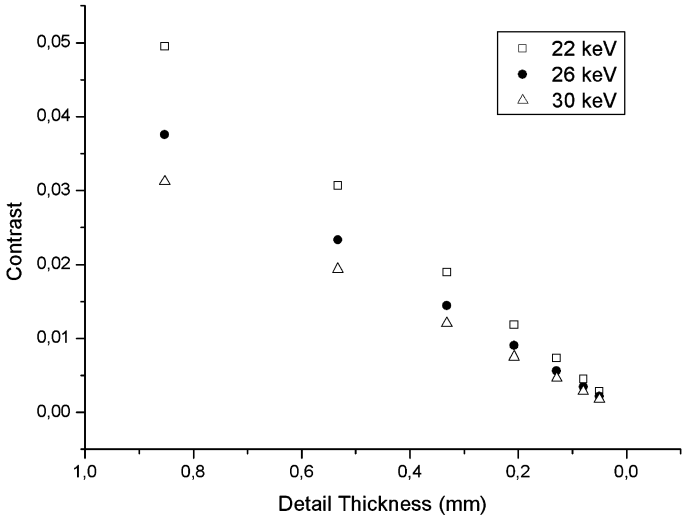

Fig. 4. – Contrast calculated from Monte Carlo data for different hole thicknesses and different energies.

fluence [13]. In all the simulations the MGD was comparable to the one imparted in a clinical examination, ranging from 1.5 to 1.8 mGy.

As the object to be imaged the Contrast Detail Phantom (CDP) for Mammography (model 18-252, Nuclear Associates, USA) was chosen. It is made of a block of Polymethyl Methacrylate (PMMA) containing several cylindrical holes of different diameter and thickness as shown in fig. 2. On the same row the hole thickness (T) was kept constant, varying hole diameter (D) while on the same column D is constant and T varies.

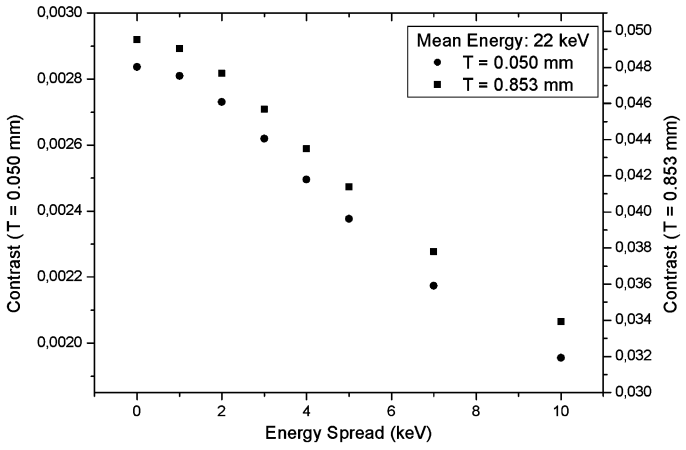

Fig. 5. – Contrast for quasi-monochromatic beam, as a function of energy spread. Contrast is reported for the thicker detail ($T = 0.853$ mm) and for the thinner detail ($T = 0.050$ mm). Mean energy is 22 keV.

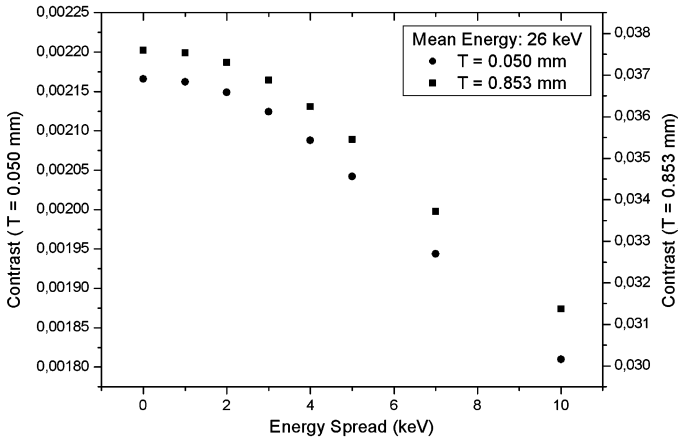

Fig. 6. – Contrast for quasi-monochromatic beam, as a function of energy spread. Contrast is reported for the thicker detail ($T = 0.853$ mm) and for the thinner detail ($T = 0.050$ mm). Mean energy is 26 keV.

To simulate PMMA, the following chemical composition was used: 0.80541 H, 0.599846 C, 0.319613 O (weight fractions). The density was supposed to be 1.19 g/cm^3. Air was composed of 0.755268 N, 0.231781 O, 0.012827 Ar and 0.000124 C, with a density of 1.22×10^{-3} g/cm^3 [14].

Instead of a single simulation for the whole phantom, we ran a simulation per each detail. For each simulation, a PMMA block of $80 \times 80 \times 45.7$ mm^3 was imaged, containing a hole of $\left(\frac{D\sqrt{\pi}}{2}\right) \times \left(\frac{D\sqrt{\pi}}{2}\right) \times T$ mm^3, where T and D take values shown in fig. 2.

The phantom was directly in contact with the detector surface and it was surrounded by an air box of $5 \times 20 \times 20$ cm^3.

The simulated detector was an ideal digital one, meaning that each energy is counted with 100% efficiency and no additional noise is added. In this way, results are general and not detector dependent. The pixel pitch of the ideal detector was 100 microns.

Only the transmitted part of the radiation was considered. In this present work, we were interested on how image quality is dependent on the X-ray source energy spectrum. Therefore, we neglected the contribution of the scattered radiation, which is strongly dependent on the imaging modality.

Image properties are evaluated in terms of contrast and signal detection properties.

Contrast is defined as the ratio of the signal difference (between object signal and a background) to the signal [15]:

$$C = \frac{n_S - n_B}{n_B} = \frac{\Delta n}{n}\,. \tag{1}$$

For a given detail, contrast C is simply a function of photon energy (or energy distribution) if noise, scattering and detector deviation from ideal behavior are not present [15]. Thus differences in contrast for the same detail are due only to spectrum differences.

For a monochromatic beam of energy E passing through a block of given material

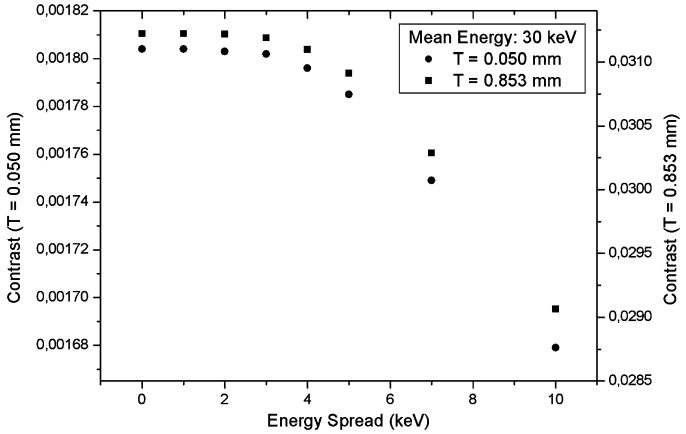

Fig. 7. – Contrast for quasi-monochromatic beam, as a function of energy spread. Contrast is reported for the thicker detail ($T = 0.853$ mm) and for the thinner detail ($T = 0.050$ mm). Mean energy is 30 keV.

containing a detail of thickness x, contrast can be easily calculated [15]:

$$C = e^{-\Delta\mu(E)x} - 1\,, \tag{2}$$

where $\Delta\mu(E)$ is the difference in absorption coefficients between detail and block materials, at energy E. For each detail of CDP, contrast was calculated theoretically considering PMMA as block material and air as detail material.

In a noisy image, object detectability depends on signal level and on object area. Rose model [16, 17] takes into account this effect in the Signal-to-Noise Ratio (SNR), defined as the ratio of signal-background difference to noise, defined as standard deviation of

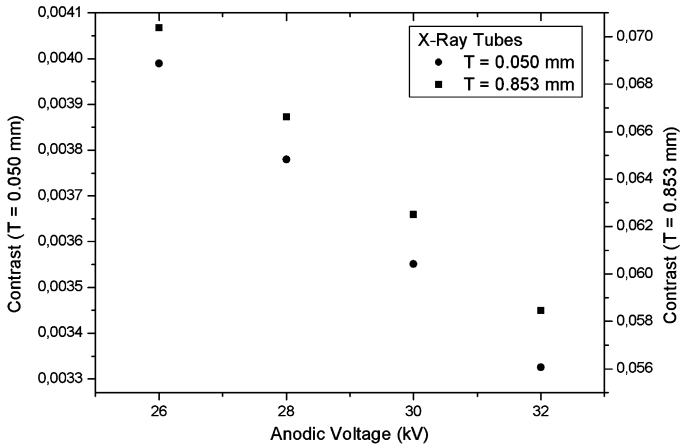

Fig. 8. – Contrast for X-ray tube beams, as a function of anodic voltages. Contrast is reported for the thicker detail ($T = 0.853$ mm) and for the thinner detail ($T = 0.050$ mm).

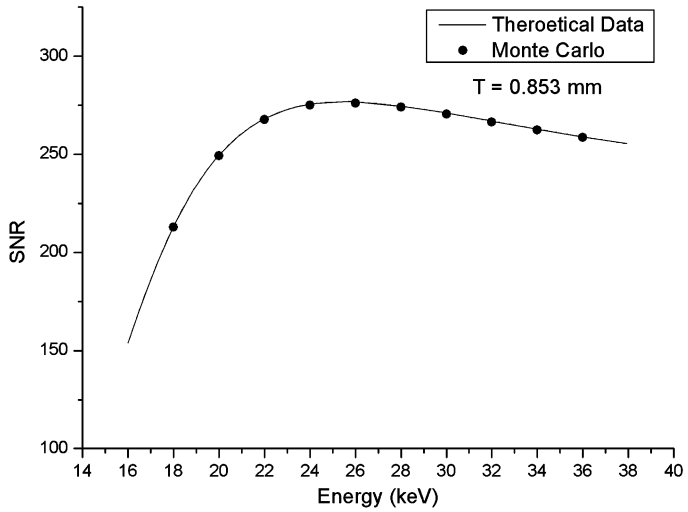

Fig. 9. – Comparison between calculated SNR and the one obtained from Monte Carlo data, for monochromatic beams, for the 0.853 mm thickness detail, as a function of energy. The diameter of the detail is $D = 4.292$ mm.

background. Signal, background and noise are evaluated on sampling areas as big as the detail to be detected is.

Regarding noise, it is supposed to follow Poisson statistics. It follows that, if signal level on a pixel is n, noise is $\sigma = \sqrt{n}$. If the sampling area A is made of N pixels, the signal is $n_A = n \cdot N$, n being the average signal on a single pixel, and noise on the area is $\sigma_A = \sqrt{n \cdot N}$ [17, 18].

The mean number of photons registered by the ideal detector in correspondence of the hole (signal) and on an equivalent area of the block (background) are used for SNR evaluation.

Hence SNR is defined as follows:

$$\text{SNR} = \frac{\Delta n_A}{\sigma_A} = \sqrt{N} \cdot \frac{\Delta n}{\sqrt{n}} = \sqrt{N} \cdot \sqrt{n} \cdot C\,, \tag{3}$$

where C is the contrast.

For comparison, SNR is also calculated directly, as done for contrast in eq. (2):

$$\text{SNR} = I_0^{1/2} e^{\frac{-(\mu_1(E)t)}{2}} \left(e^{-\Delta\mu(E)x} - 1\right)\,, \tag{4}$$

where $\Delta\mu(E)$ is the difference in absorption coefficients between detail and block materials, at energy E, μ_1 is the absorption coefficient of the block material, t is the thickness of the block, x the thickness of the detail and I_0 is the number of photons impinging on the detail.

Generally, a detail is considered visible if SNR is greater than 5 [16]. Even though defining a threshold value for visibility is in some way arbitrary, the parameter can certainly be used to compare different imaging techniques for the same detail. In this

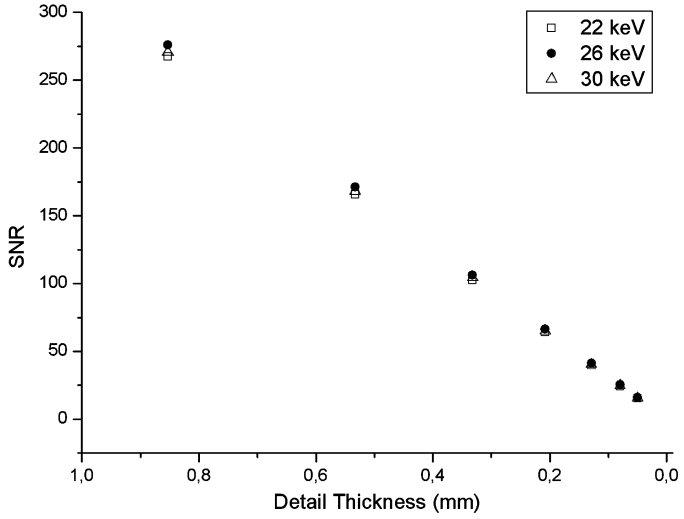

Fig. 10. – SNR calculated from Monte Carlo data as a function of different hole thicknesses and different energies. The diameter of the details is $D = 4.292$ mm.

paper, this threshold is used to define if a given detail is visible or not and the number of visible details is used as a scoring method for different energy spectra.

3. – Results

For monochromatic beams a comparison of contrast data obtained by Monte Carlo simulation and calculated contrast was performed. For a theoretical calculation eq. (2)

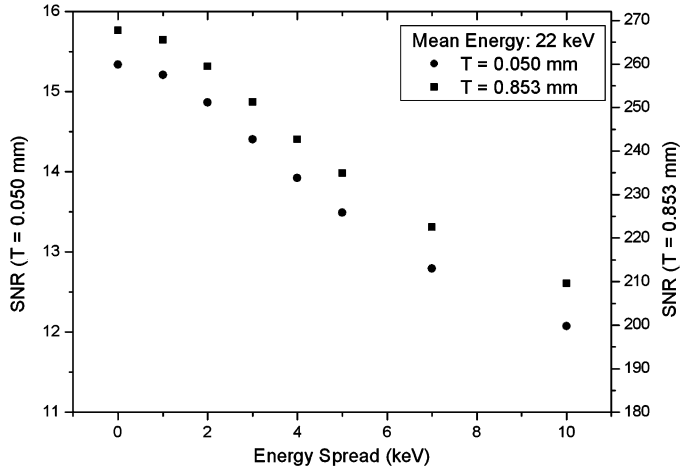

Fig. 11. – SNR for quasi-monochromatic beam, as a function of energy spread. SNR is reported for the thicker detail ($T = 0.853$ mm) and for the thinner detail ($T = 0.050$ mm). Mean energy is 22 keV. The diameter of the details is $D = 4.292$ mm.

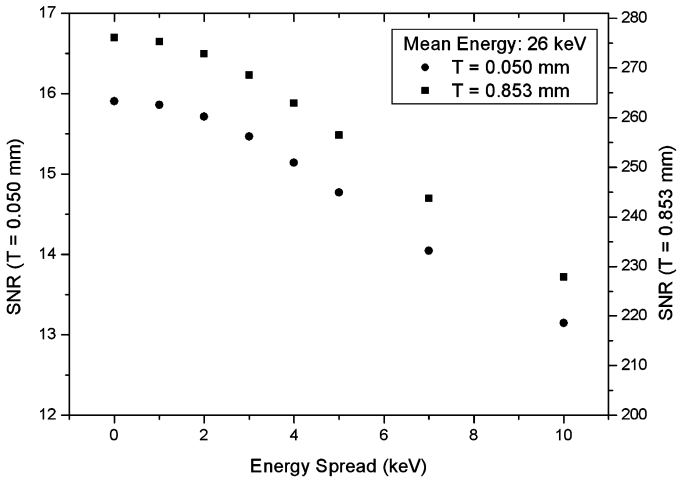

Fig. 12. – SNR for quasi-monochromatic beam, as a function of energy spread. SNR is reported for the thicker detail ($T = 0.853$ mm) and for the thinner detail ($T = 0.050$ mm). Mean energy is 26 keV. The diameter of the details is $D = 4.292$ mm.

was used and absorption coefficients data were those provided by XCOM database [14]. Results are presented in fig. 3, for the detail of thickness $T = 0.853$ mm. As can be noted, the agreement is good. The decrease in contrast, as a function of energy, was about 65%, ranging from 0.075 at 18 keV to 0.026 at 36 keV. The same percentage decrease was obtained for the thinnest detail ($T = 0.05$ mm), where contrast ranged from 0.0042 at 18 keV to 0.0015 at 36 keV.

In fig. 4, the dependence of contrast on detail thickness is shown, for three different energies: 22, 26 and 30 keV. We chose these energies since 26 keV is the energy at which the SNR presents a maximum (see below) and 22 and 30 keV are equidistant from this maximum. For each energy, the contrast decreased by 94% as a function of detail thickness, from $T = 0.853$ mm to $T = 0.050$ mm. For each detail thickness, the contrast variation from 22 keV to 30 keV was about 37%.

These energies have been used as mean energies for the simulations of quasi-monochromatic beams: results are presented in figs. 5, 6 and 7, for 22, 26 and 30 keV, respectively. In each figure the contrast for the thicker and the thinner detail is shown, as a function of energy spread (standard deviation), ranging from 1 to 10 keV. The contrast reduction was less than 1% for $\sigma = 1$ keV, less than 10% for $\sigma = 3$ keV and reached 30% at $\sigma = 10$ keV, for mean energy 22 keV. The reduction was less than 1% for $\sigma = 2$ keV, less than 10% for $\sigma = 5$ keV and reached 16% at $\sigma = 10$ keV, for mean energy 26 keV. he contrast reduction was less than 1% up to $\sigma = 4$ keV and less than 10% up to $\sigma = 10$ keV for mean energy 30 keV.

In fig. 8, the same data are presented for the X-ray tube spectra.

Since the main energy of tube spectra is comprised between 16 an 18 keV, contrast for these spectra is generally high, even if it is lower than the contrast for the monochromatic beam at 18 keV (see fig. 3). This is due to the large energy spread of X-ray tubes. For example, considering the thicker detail contrast for the tube spectra at 32 kV of anodic voltage (whose mean energy is 17.2 keV) is 20% lower than the contrast for 18 keV monochromatic beam.

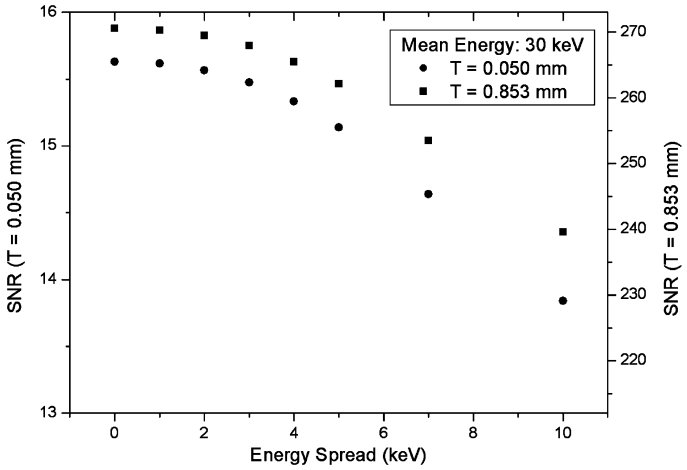

Fig. 13. – SNR for quasi-monochromatic beam, as a function of energy spread. SNR is reported for the thicker detail ($T = 0.853$ mm) and for the thinner detail ($T = 0.050$ mm). Mean energy is 30 keV. The diameter of the details is $D = 4.292$ mm.

Regarding quasi-monochromatic beams, results show that a small energy spread does not affect significantly the contrast: a 2 keV energy spread produces in the worst case (*i.e.* mean energy 22 keV) a contrast degradation of 4%.

SNR results are presented here for the details having the larger area ($D = 4.292$ mm, first column of fig. 2). Data for the other columns can be easily obtained by scaling these results by the ratio of the square roots of the detail areas, as can be derived by eq. (3).

In fig. 9, a comparison of SNR data for monochromatic beams obtained by Monte Carlo simulation and calculation from eq. (4), for the most visible detail ($T = 0.853$ mm)

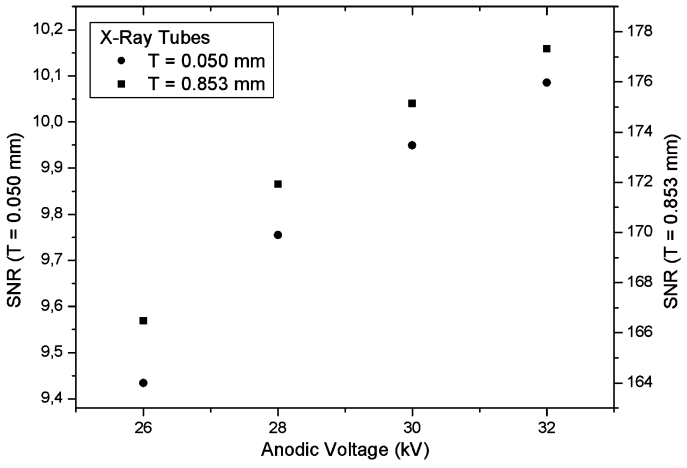

Fig. 14. – SNR for X-ray tube beams, as a function of anodic voltages. SNR is reported for the thicker detail ($T = 0.853$ mm) and for the thinner detail ($T = 0.050$ mm). The diameter of the details is $D = 4.292$ mm.

TABLE I. – *Visibility scores for monochromatic beams.*

Energy (keV)	Visible details	Energy (keV)	Visible details
18	35	28	38
20	37	30	38
22	38	32	38
24	38	34	38
26	39	36	38

is presented. As can be seen, there is a maximum in SNR at 26 keV and SNR decreases more steeply moving from the maximum towards lower energies than moving from the maximum towards higher energies. The largest variation in SNR (23%) is between 26 keV and 18 keV, while the SNR decrease from the maximum up to 30 keV is about 6%. This maximum is at the same energy also for the other detail thicknesses and the energy dependence is of the same type of that shown in fig. 9. Also for SNR the agreement between MC and calculated data is good.

Figure 10 presents the dependence of SNR on detail thickness for the three energies used above. The decrease of SNR is 94% from $T = 0.0853$ mm to $T = 0.050$ mm, for each energy.

Figures 11, 12 and 13 present SNR for the quasi-monochromatic beams of mean energy 22, 26 and 30 keV, respectively. Image quality is not dramatically affected by energy spread of quasi-monochromatic beams: SNR reduction is less than 1% at an energy spread of 1, 2 and 3 keV, less than 10% at an energy spread of 4, 5 and 7 keV for mean energies 22, 26 and 30 keV respectively, with respect to the corresponding monochromatic energy.

TABLE II. – *Visibility scores for quasi-monochromatic beams.*

$E = 22$ keV		$E = 26$ keV		$E = 30$ keV	
DE (keV)	Visible details	DE (keV)	Visible details	DE (keV)	Visible details
0	38	0	39	0	38
1	38	1	39	1	38
2	38	2	38	2	38
3	37	3	38	3	38
4	36	4	38	4	38
5	36	5	37	5	38
7	36	7	36	7	37
10	35	10	36	10	37

TABLE III. – *Visibility scores for X-ray tubes beams.*

Anodic voltage (kV)	Visible details
26	33
28	33
30	34
32	34

Figure 14 presents results for the four tube spectra: SNR increases with the mean energy of the spectrum, since the mean energy is always lower than 20 keV. However, for these spectra SNR is significantly lower than those for monochromatic and quasi-monochromatic energy distributions: the difference between the best SNR for X-ray tubes (177 for 32 kV) and the best SNR for monochromatic beams (276 for 26 keV) is 36%.

In tables I, II and III, the number of visible (SNR $\geqslant 5$) details of the phantom is reported for each energy spectrum. The greatest number of details (39) is visible for 26 keV of mean energy, up to 1 keV of energy spread. 38 details are visible up to 2 of energy spread for mean energy 22 keV, up to 4 keV for 26 keV and up to 5 keV for 30 keV. For X-ray tubes, the highest number of visible details is 34 and it is obtained at 32 kV.

4. – Conclusion

Presented results confirm the advantage (in terms of contrast and SNR) of using monochromatic instead of polychromatic sources.

These results also indicate that Thomson back-scattering sources with an energy spread of 1–2 keV can be a promising alternative to traditional X-ray tubes in mammography. With regard to Contrast Detail Phantom, contrast obtained by a quasi-monochromatic source is of the same order of that obtained by monochromatic beams and significantly higher than that obtained by traditional polychromatic sources. As an example, an energy spread of 2 keV generates a decrease of contrast of about 4% and a loss of SNR of about 3% in the worst case (mean energy 22 keV) if compared to the same quantities for the monochromatic beam of the same energy.

Detail visibility is higher for Thomson back-scattering sources than for X-ray tubes. For example, if we compare the image (detail thickness $T = 0.0853$ mm) obtained using tubes at an anodic voltage of 30 kV and the one using the quasi-monochromatic sources with mean energy 26 keV and 1 keV of energy spread, we obtain an increase of SNR of 57%, compared to a decrease of contrast of 40%. This implies that small (or fancy) details not visible for traditional tubes appear in Thomson back-scattering generated images. On the other hand, the same detail visibility can be achieved with a lower fluence.

All conclusions reached in this paper concern CDP, that is made of PMMA and air. However, breast chemical composition is different from PMMA [19, 20] and these results may vary, in particular concerning the energy at which SNR presents a maximum. For example, the best energy to image the CDP is 26 keV, that appears to be slightly higher than typical energies used in mammography (20 keV).

Therefore, better considerations on improvement due to the use of quasi-monochromatic sources in mammography have to deal with breast (or breast-like phantoms) imaging.

REFERENCES

[1] Ragozzino M. W., *Med. Phys*, **9** (1982) 493.
[2] Cranley K., Gilmore B., Fogarty G. and Desponds L., *Catalogue of diagnostic X-ray spectra and other data* , IPEM Report 78 (IPEM, York).
[3] Moeckli R., Verdun F. R., Fiedler S., Pachoud M., Schnyder P. and Valley J., *Phys. Med. Biol.*, **45** (2000) 3509.
[4] Arfelli F. *et al.*, *Phys. Med. Biol.*, **43** (1998) 2845.

[5] Bravin A., *J. Phys. D*, **36** (2003) 24.
[6] Katsuhiro Dobashi *et al.*, *Development of compact hard X-ray source based on laser-electron collision using x-band linac, Proceedings of EPAC 2002, Paris, France.*
[7] Tomassini P. *et al.*, *Phys. Plasmas*, **10** (2003) 917.
[8] Alesini D. *et al.*, *The Project PLASMONX for Plasma Acceleration Experiments and a Thomson X-Ray Source at SPARC, Proc. PAC-2005, Knoxville (USA), May 16-20 2005*, IEEE Cat. n. 05CH37623C, ISBN 0-7803-8860-7, p. 820.
[9] Bottigli U., Brunetti A., Golosio B., Oliva P., Stumbo S., Vincze L., Randaccio P., Bleuet P., Simionovici A. and Somogyi A., *Spectrochimica Acta Part B: Atomic Spectroscopy*, **59** (2004) 1747.
[10] Doster M. and Gardner P., *X-ray Spectrom.*, **11** (1982) 173.
[11] Doster M. and Gardner P., *X-ray Spectrom.*, **11** (1982) 181.
[12] Boone M. J., *Med. Phys.*, **29** (2002) 869.
[13] Boone M. J. and Seibert J. A., *Med. Phys.*, **24** (1997) 1661.
[14] Berger M. J. and Hubbell J. H., 1987 *XCOM: Photon Cross Sections on a Personal Computer, NBSTIR 87-3597* (National Institute of Standards and Technology, Gaithersburg, MD), `http://physics.nist.gov/PhysRefData/Xcom/Text/XCOM.html`.
[15] Webb S. (Editor), *The Physics of Medical Imaging* (IOPP, Bristol) 1988, ISBN 0-85274-349-1.
[16] Rose A., *Vision: Human and Electronic* (Plenum, New York) 1973.
[17] Wagner R. F., *Med. Phys*, **4** (1977) 279.
[18] Dainty J. C. and Shaw R., *Image Science* (Academic Press, London) 1974.
[19] Hammerstein G. R., Miller D. W., White D. R., Masterson M. E., Woodard H. Q. and Laughlin J. S., *Radiology*, **130** (1979) 485.
[20] Poletti M. E., Gonçalves O. D. and Mazzaro I., *Phys. Med. Biol.*, **47** (2002) 47.